Domain formation in arrays of square holes in an Fe film

I. Guedes* and M. Grimsditch
Material Science Division, Argonne National Laboratory, Argonne, Illinois 60439

V. Metlushko
Department of Electrical Engineering and Computer Science, University of Illinois at Chicago, Chicago, Illinois 60607

P. Vavassori
INFM, Dipartimento di Fisica, University of Ferrara, Ferrara, Italy

R. Camley†
Physics Department, University of Colorado, Colorado Springs, Colorado 80933-7150

B. Ilic
School of Applied and Engineering Physics, Cornell University, Ithaca, New York 14853

P. Neuzil and R. Kumar
Institute of Microelectronics, 11 Science Park Road, 117685, Singapore
(Received 7 February 2001; revised manuscript received 1 March 2002; published 19 July 2002)

Domain formation during magnetization reversal in arrays of square holes in Fe films is investigated using the diffracted magneto-optic kerr effect (DMOKE). The shape of the domains can, in some cases, be extracted from hysteresis loops measured at various diffraction orders. We find that the shape of the domains depends strongly on: the direction of the applied field relative to the holes, the size of the square holes, and also the small intrinsic anisotropy of the unpatterned film. DMOKE results are compared with those obtained with magnetic force microscopy. In the saturated state Brillouin spectroscopy shows that square holes induce a fourfold anisotropy in the film.

DOI: 10.1103/PhysRevB.66.014434 PACS number(s): 78.20.Ls, 75.60.Jk, 75.30.Gw

Relatively little is known about the behavior of magnetic nanoarrays of holes. Most investigations to date have relied on micromagnetic calculations and magnetic force microscopy (MFM).[1–6] In two recent investigations,[7,8] we have shown that diffracted magneto-optic kerr effect (DMOKE) is also a very powerful tool to study domain formation during the magnetization reversal. In Ref. 7, we discussed qualitatively how the DMOKE loops were consistent with blade domains forming around circular holes in the film. In Ref. 8, we presented a mathematical formalism that allowed a more quantitative analysis of the DMOKE loops. This formalism, applied to an array of elliptical holes[8] with applied fields perpendicular to the long axis of the ellipses, showed that 90° domains, that bridge next-nearest neighboring holes, are formed during the switching process.

Here we apply the formalism developed in Ref. 8 to investigate the domains in arrays of square holes. We find that the nature of the domains depend on: the direction of the applied field relative to the squares, the size of the square holes, and on the intrinsic anisotropy of the unpatterned film.

We have also used Brillouin scattering to characterize the magnetic properties of arrays. The frequencies of the magnetic excitations studied with this technique are determined by the magnetization, the anisotropies, and the applied field. Magnon frequencies measured as a function of in-plane propagation direction in the saturated state (viz., constant field and magnetization) provide a direct probe of the anisotropy. Here we show that an array of square holes induces a fourfold anisotropy in the film. Since similar experiments on circular[7] and elliptical[8] hole arrays showed no anisotropy and a twofold anisotropy, respectively, we conclude that the origin of the anisotropy is the shape of the holes and not the symmetry of the lattice.

Micromagnetic calculations and MFM studies have also been carried out on our arrays of holes. The difficulties encountered with these techniques will be briefly discussed and a few relevant results are presented.

I. EXPERIMENTAL DETAILS

The fabrication techniques and DMOKE system used for the experiments are identical to those described in Refs. 7 and 8. In the present case, 60-nm-thick Fe films with a 2.5-nm Cr overlayer (to prevent oxidation) were patterned with square holes on a 1×1 μm lattice. Scanning electron microscopy (SEM) images of the two samples investigated are shown in Fig. 1.

MOKE loops were recorded in what is known as the ''transverse MOKE'' configuration; the applied field is perpendicular to the plane that contains both the direction of incident light and the surface normal. Only the intensity of the reflected light is monitored (i.e., no analyzer is used in the reflected beam). This configuration is sensitive only to the component of magnetization M perpendicular to the plane of incidence. The DMOKE loops presented here were all obtained on diffracted beams in the plane of incidence. The interpretation of loops obtained on out-of-plane diffracted beams is complicated due to polarization mixing and sensitivity to other components of M.

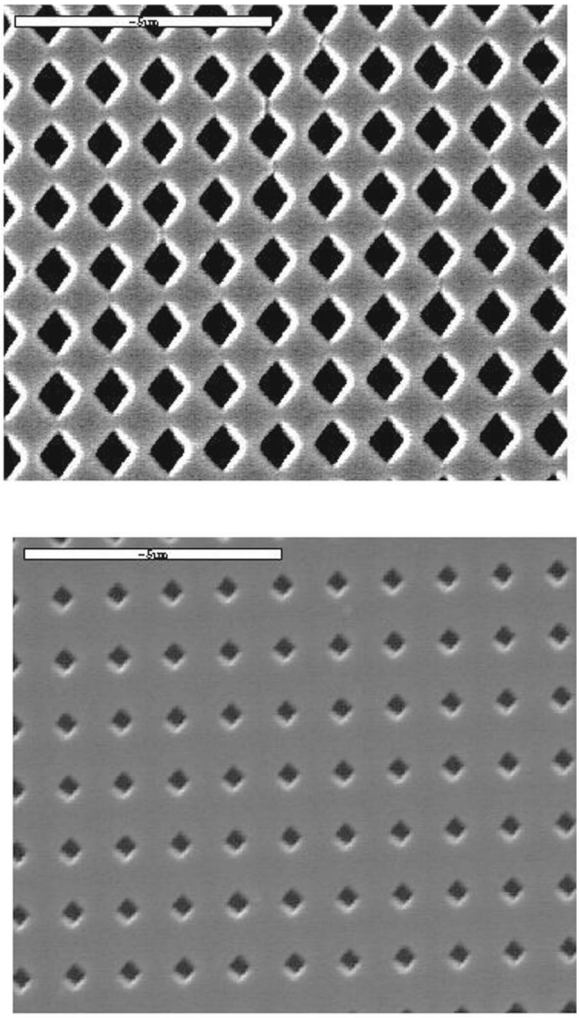

FIG. 1. SEM images of the two arrays of square holes in an Fe film investigated here.

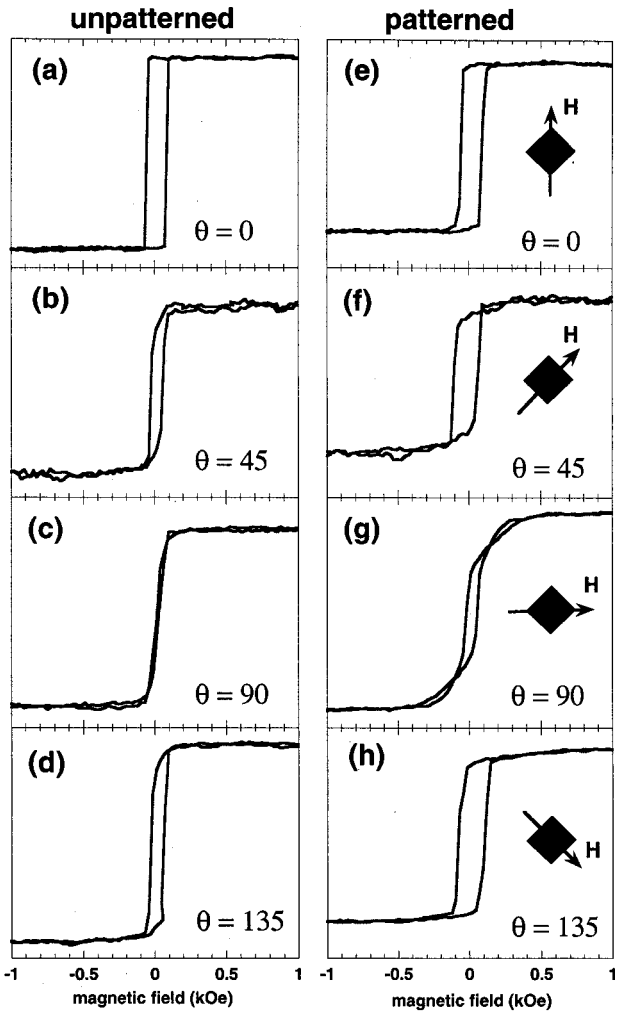

FIG. 2. Angle dependence of Moke hysteresis loops on the unpatterned area (a)–(d) of the array of small squares. For $\theta = 0$, the magnetic field is applied along the diagonal of the square holes. Moke hysteresis loops measured on the reflected spot from the patterned area (e)–(h) of the film.

Our Brillouin spectra were obtained on a $5+4$ pass tandem Fabry Perot interferometer.[9] The Brillouin technique measures excitations that are very closely related to the modes detected in ferromagnetic resonance experiments. Since the frequency of these modes depends on the magnetization and anisotropies, they are used to probe the contributions to the magnetic energy.

MFM investigations were performed on a digital nanoscope III instrument with an applied external field generated by a pair of Helmholtz coils.

Micromagnetic calculations were performed using the web version of the NIST code.[10]

II. RESULTS: MOKE AND BRILLOUIN

Figures 2(a)–2(d) show the hysteresis loops obtained on the unpatterned portion of the sample with small square holes [Fig. 1(b)]. (The angles in the figure indicate the field direction relative to one axis of the array.) These loops clearly show that the as-deposited film has a uniaxial anisotropy with a hard axis along the 90° direction. This anisotropy is not uncommon in thin films and most likely develops during the film deposition process either due to the influence of the substrate or due to off-normal deposition.

Figures 2(e)–2(f) show hysteresis loops recorded from the patterned area using the reflected (i.e., zeroth-order diffracted) beam. As discussed in Ref. 8 the zeroth-order loops yield the average magnetization as expected for conventional MOKE measurements. Although the 0° and 90° directions should be equivalent with respect to the array symmetry, the 0° and 90° loops are quite different. However, as for the unpatterned area, the loops show that 90° is still a hard axis.

The anisotropy of the sample in Fig. 1(b) was also investigated using Brillouin scattering. The Brillouin spectra exhibit two magnons peaks similar to those discussed in Ref. 8. In the unpatterned area these peaks correspond to surface and standing spin-wave excitations. In the patterned area the Brillouin spectra are very similar, indicating that the excitations are not very different from those in the unpatterned area. In Fig. 3, we plot the frequencies of the two modes as a function of the angle between the applied field and one of

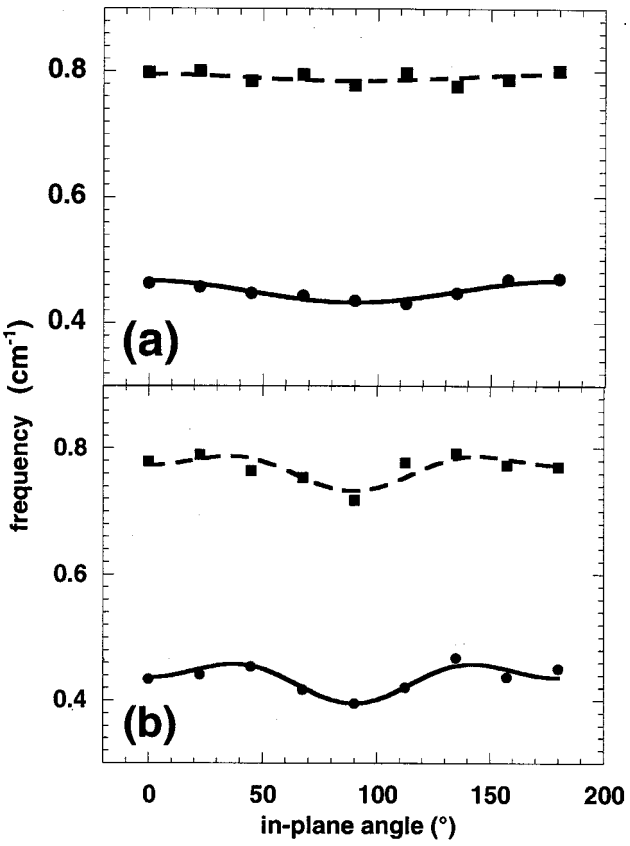

FIG. 3. Magnon frequencies in the (a) unpatterned and (b) patterned areas versus in-plane angle. In these measurements $H = 0.5$ kOe. Squares and circles indicate the surface and standing-wave modes, respectively.

the array axes for a field of 0.5 kOe: in Fig. 3(a) for the unpatterned area and in Fig. 3(b) for the patterned area. The dip observed in the lower mode in Fig. 3(a) is consistent with a hard axis along the 90° direction. The full and dashed lines are fits to $\omega = \omega_0 + \Delta\omega_1 \sin^2(\theta)$; where $\Delta\omega_1$ is proportional to the anisotropy. The data in Fig. 3(b) clearly show evidence of a fourfold anisotropy induced by the hole array. The data have been fitted with $\omega = \omega_0 + \Delta\omega_1 \sin^2(\theta) + \Delta\omega_2 \sin^2(2\theta)$, where $\Delta\omega_1$ and $\Delta\omega_2$ reflect the uniaxial and fourfold anisotropies. A quantitative estimate of the anisotropies requires a theory of magnon modes in hole arrays; such a theory has not yet been developed. It is interesting to note that although the fourfold anisotropy is clearly evident in the Brillouin data, it is not clearly apparent in the magnetization data in Fig. 2.

We were unable to obtain Brillouin data on the sample with large holes [Fig. 1(a)]. Presumably this is due to the decrease in the amount of magnetic material, which reduces the signal and leads to very low quality spectra.

The existence of a fourfold anisotropy induced by the square holes, with the easy axes along the diagonals, is somewhat unexpected because, in a fully saturated state, a magnetic square is expected to be isotropic. However, isotropy in the saturated state results from the dipolar energy contributions from the edges being the same for any direction of magnetization. Below saturation small, inhomogeneous reorientations of the magnetization by an angle ϕ in the vicinity of the hole produce an increase in exchange energy proportional to ϕ^2. However, the reduction in dipolar energy is proportional to ϕ^2 when M is perpendicular to the edge but linear in ϕ when M is at 45° to the edge. These small deviations from the saturated state, lead to a lower total energy when the field is along the diagonal. The above discussion is easily verified with micromagnetic calculations.

III. RESULTS: DMOKE

Figure 4 shows DMOKE loops measured on various diffraction orders on the sample with small squares and for in-plane angles 0°, 45°, and 90°, respectively. The 135° loops are very similar to those at 45° and are not shown. As discussed in Ref. 8, the differences between the loops measured on different diffraction orders reflect the effect of domain formation. In Ref. 8, it was shown that these changes can be viewed as originating from the changes in the magnetic form factor defined by

$$f_p = \int_s m_y \exp(in\,\mathbf{G}r)\,dS, \tag{1}$$

where $\mathbf{G} = 2\pi/a$, a is the lattice constant of the array, n is the diffraction order, and the integral is carried out over a unit cell of the array. Because of the limited number of diffraction orders that can be accessed, it is not possible to use the methods typically used in x-ray or neutron diffraction to extract the spatial dependence of m_y within the unit cell. It is possible, however, to use Eq. (1) to determine if an *ad hoc* domain configuration is consistent with the measured DMOKE loops. For most of the structures and field directions investigated here, we were able to find domain configurations that are, simultaneously, energetically reasonable and consistent with the magnetization loops.

The treatment given in Ref. 8 of how the DMOKE loops are related to the magnetic form factor, does not include a discussion of complex form factors. However, since the domains reported in Ref. 8 preserved the inversion symmetry of the unit cell, the imaginary part of the form factors are zero and hence played no role. In the present investigation some of the domain structures that are invoked to explain the experimental results do break the inversion symmetry and hence lead to complex form factors. For the results to be presented here, the effects of complex form factors are small and consequently cannot be reliably discussed. A full discussion of this topic will be presented elsewhere but we anticipate here that the DMOKE signal (I) takes on the form

$$\mathrm{I} \quad \propto \quad K' \,\mathrm{Re}[f_p] \pm K'' \,\mathrm{Im}[f_p], \tag{2}$$

where K' and K'' are functions of the complex magneto-optic coupling constant, complex dielectric constant, and angle of incidence. Theoretical estimates for Fe indicate that $K'/K'' \sim 10$. For the structures to be discussed here, the neglect of the imaginary part appears to be justified.

In principle, the field-dependent form factors can be extracted from micromagnetic simulations and, via Eq. (2), the corresponding DMOKE loops are evaluated. However, as

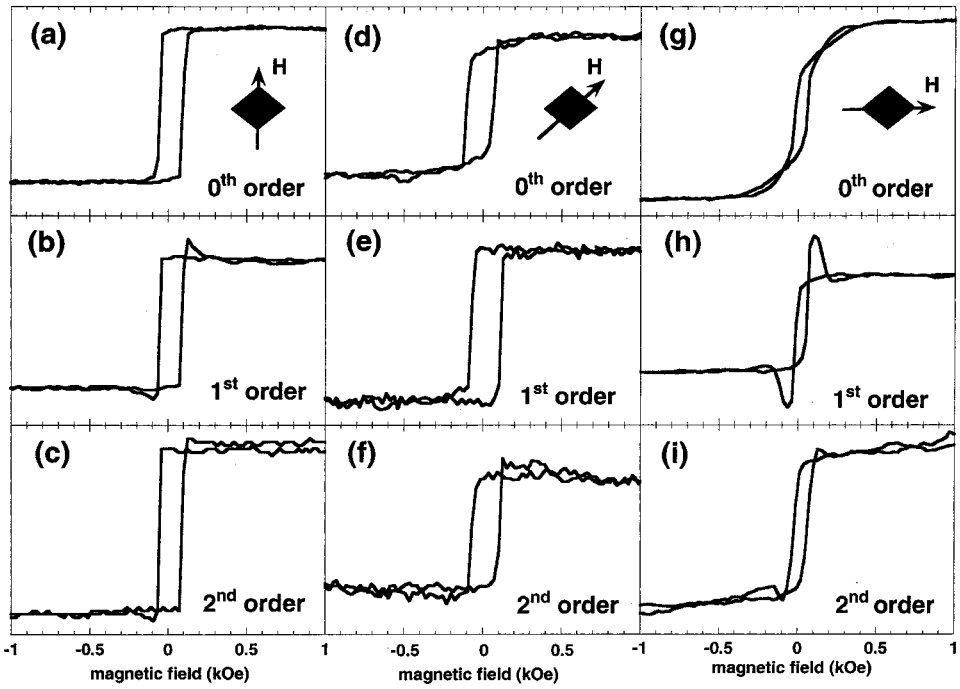

FIG. 4. DMOKE hysteresis loops of various orders from the patterned area of the array of small squares. (a)–(c):H parallel to hole diagonal ($\theta=0°$), (d)–(f):H parallel to edge ($\theta=45°$), and (g)–(i):H parallel to other diagonal ($\theta=90°$).

will be described in the following section, edge effects make this approach nontrivial to implement.

In lieu of the above more rigorous description it is possible to obtain some insight into the domain formation by constructing plausible domains and checking to see if they produce qualitative agreement with the measured loops. There are two energy-related constraints that we have used to construct possible domain structures. Both are based on dipolar magnetostatic energy contributions. To minimize dipolar energy there is a driving force to align the magnetization parallel to any free surface, viz., the edges of holes. Also, to eliminate dipolar fields at domain boundaries, domain walls tend to be perpendicular to the bisector of the two adjacent magnetization directions thereby eliminating charges on the domain wall. For a square hole magnetized parallel to an edge these considerations lead to the domain pattern shown in Fig. 5(a) (or its symmetry-equivalent configuration). For a single hole this pattern requires infinite domain-wall energy so that the system relaxes by a trade-off between wall and dipolar energies leading to domains schematically shown in Fig. 5(b). These type of domains are well known[11–13] and are conventionally called blade domains. Their observation in an array of circular holes was reported in Ref. 7. In the present context the length of the blades is the only parameter that can be adjusted to produce agreement with experimental data.

When the same hole is magnetized along a diagonal the two domain structures shown in Figs. 5(c) and 5(e) satisfy the energy conditions described above. The configuration in Fig. 5(c) can reduce its domain-wall energy by developing blade domains like those in Fig. 5(d). The configuration in Fig. 5(e), on the other hand, does not have that flexibility and hence is energetically forbidden for a single hole. As we will show, however, in an array of holes, it remains an energetically viable domain structure.

Figure 6 contains schematics of possible domains in our array of small square holes for two field directions. Although these figures are obvious generalizations of the domains shown in Fig. 5, it is also clear that the generalizations are not unique. For example, the ''blades'' in Fig. 5(b) could be chosen to be shorter and not overlap as in Fig. 6(a). The domains in Fig. 6 were chosen, as outlined below, to yield qualitative agreement with the experimental data in Fig. 4. The form factors for the saturated and the ''domain'' states shown in Fig. 6 are given in Table I. As discussed in Ref. 8 the ratio of the hysteresis signal at full domain formation to

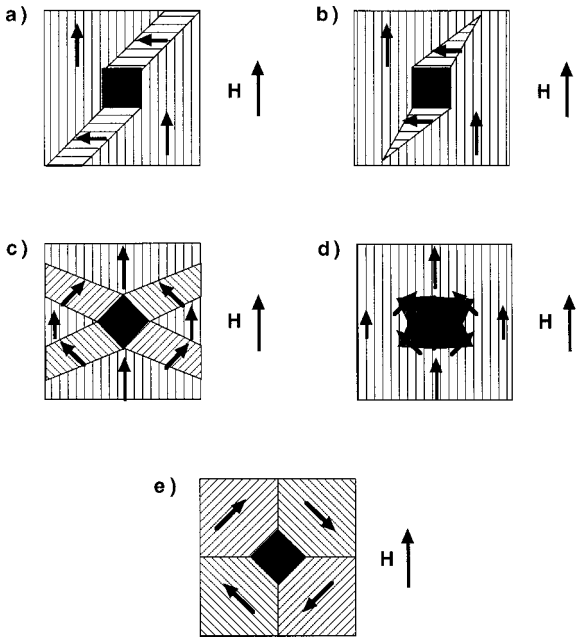

FIG. 5. Schematic diagrams of domains around square holes for two field directions. These domains eliminate all ''magnetic charges'' at the hole edges. a, c, and e also have no net charge on the domain walls. b and d represent a trade-off of wall and dipolar energies of the structures in a and c, respectively.

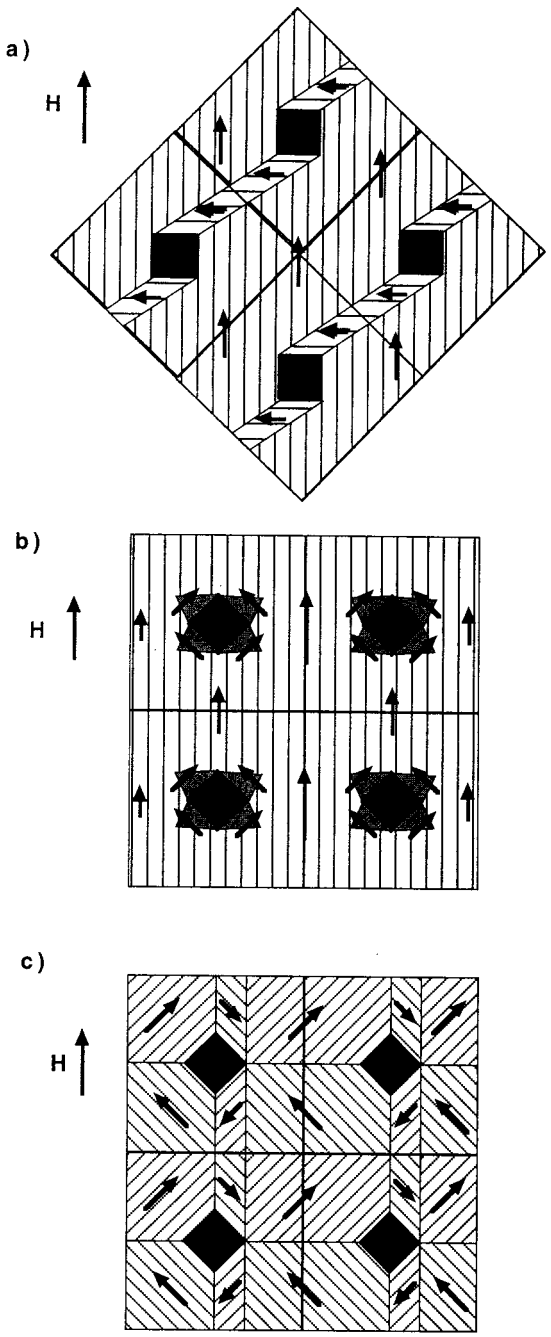

FIG. 6. Energetically viable domain structures near remanence for two directions of the applied field for the sample with small holes.

that at saturation is given by $f(\text{domain})/f$ (saturation). Thus, the form factors in rows 1 and 2 of Table I predict signal drops of 18% and 15% in the zeroth- and first-order loops and a 14% increase in the second-order loops. For the zeroth- and second-order loops this is consistent with the experimental results in Figs. 4(d) and 4(f). Agreement for the first-order loop [Fig. 4(e)] is less satisfactory, but we were unable to find any variation of the domain structure (viz., length of blade domains) that would improve the agreement.

Since the micromagnetic and MFM results, to be shown later, provide support for the domain structure in Fig. 6(a), the discrepancy between the calculated and the measured first-order form factors must therefore be attributed to the simplicity of the model. Recall that the model assumes that the same domain pattern exists in every cell and does not allow for gradual bending of the magnetization (i.e., domain walls are assumed to be infinitely narrow and only two or three possible alignment directions are allowed).

TABLE I. Form factors for the diagrams shown in Fig. 6.

	f_0	f_1	f_2
Fig. 6(a) at saturation	0.91	-0.067	-0.014
Fig. 6(a)	0.75	-0.057	-0.016
Figs. 6(b) and 6(c) (saturation)	0.91	0.080	-0.049
Fig. 6(b)	0.88	0.095	-0.043
Fig. 6(c)	0.40	$0.22+0.15i$	$-0.050-0.17i$

When the field is applied along a diagonal of the square holes the most surprising experimental result is that the loops in Figs. 4(a)–4(c) and 4(g)–4(i), that should be equivalent by symmetry, are very different. The origin for the difference may lie in the two possible energetically reasonable domain structures shown in Figs. 6(b) and 6(c). The relevant form factors are given in rows 3–5 of Table I. By making the blade domains in Fig. 6(b) small, we qualitatively reproduce the loops in Figs. 4(a)–4(c): i.e., small differences in the form factors of rows 3 and 4 correspond to only weak features in all the loops. No generalization of ''bladelike'' domains produced form factors that would even remotely explain the loops in Figs. 4(g)–4(i). However, the domain structure in Fig. 6(c) does produce good agreement. In this

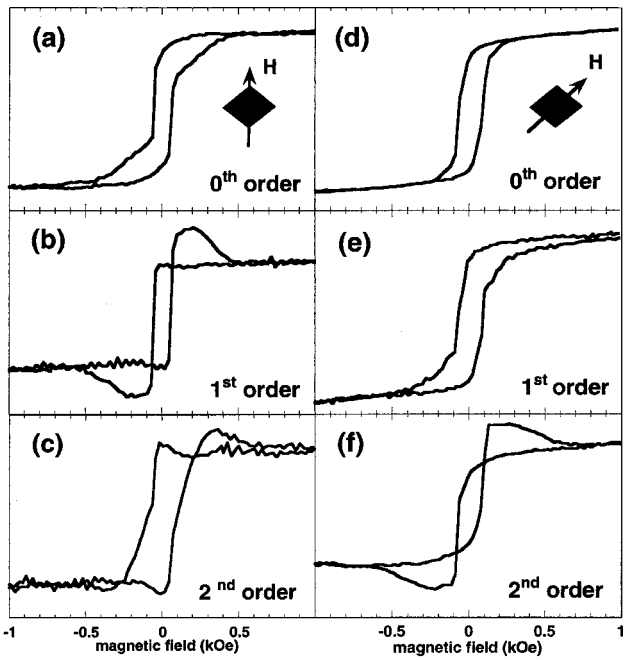

FIG. 7. DMOKE hysteresis loops of various orders from the patterned area of the array of large squares. (a)–(c), for a field along the hole diagonal ($\theta=0°$). (d)–(f), for a field parallel to an edge ($\theta=45°$).

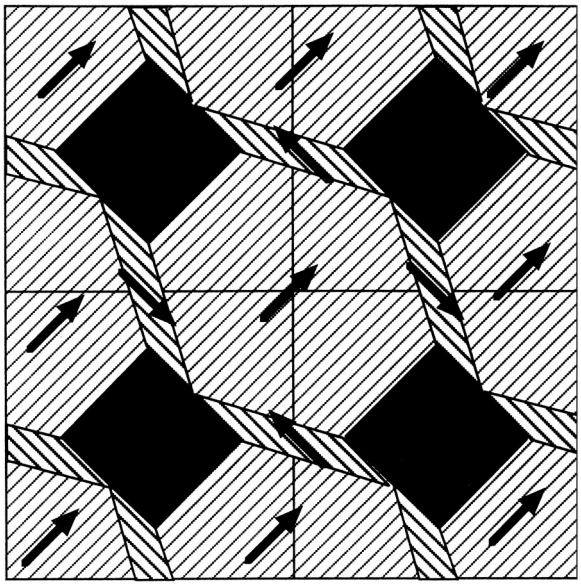

FIG. 8. Schematic diagram of domains in the array of large square holes that are consistent with the loops in Fig. 7.

case the form factors f_1 and f_2, given in row 5 of Table I, are complex due to the loss of inversion symmetry of the domain structure. Since, based on the arguments given above, the imaginary parts of the form factors contribute a factor of $\approx$10 times less than the real part, they can be neglected in the first approximation. The form factors in row 5 of Table I predict a 55% decrease in the zeroth-order loop, a 130% increase in the first-order loop, and a 16% increase in the second-order loop. These values are in good qualitative agreement with the corresponding -60%, $+80\%$, and $+10\%$ changes obtained from the loops in Figs. 4(g)–4(i). The reason for the different behavior displayed in Fig. 4 for the two equivalent directions of H can be traced to the anisotropy of the unpatterned film. This anisotropy favors domain formation [Fig. 6(c)] when the field is applied along the hard axis [Figs. 4(g)–4(i)] and hinders their formation when applied along the easy axis [Figs. 4(a)–4(c) and 6(b)].

It has been suggested that the above, very qualitative, approach could be improved and made more quantitative by fitting the measured intensity changes to the form factors obtained as a function of domain shape or size. However, in view of the simple nature of the model and the fact that it is likely that reliable form factors will soon be available from micromagnetic simulations, we have not attempted to implement such a scheme.

Figure 7 shows the experimental hysteresis loops obtained on the sample with large square holes [Fig. 1(a)] for two directions of the applied field. In this case we show only two field directions, since there are only slight differences between symmetry-equivalent directions of the array (i.e., the intrinsic anisotropy of the unpatterned film plays a less significant role). When the field is applied along the edge of a hole [Figs. 7(d)–7(f)] it is somewhat surprising that the domains in Fig. 6(a), that describe the results for the small

TABLE II. Form factors for the domain structure in Fig. 8.

	f_0	f_1	f_2
Fig. 8 @ saturation	0.81	−0.092	0.035
Fig. 8	0.64	−0.050	0.044

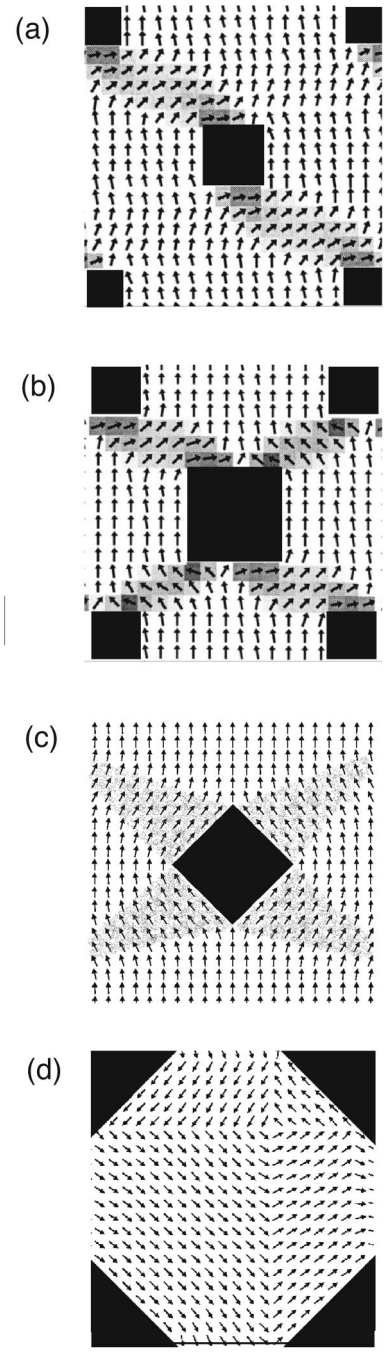

FIG. 9. Magnetization profiles obtained from micromagnetic calculations. a and c were calculated for small squares and are consistent with the domains proposed in Figs. 6(a) and 6(b). b and d were obtained on runs for large squares; the one in b is consistent with the domains proposed in Fig. 8, the schematic in d is reminiscent of the pattern proposed for the small squares in Fig. 6(c). The shaded areas were included as guides to the eye of the regions with rotated magnetizations.

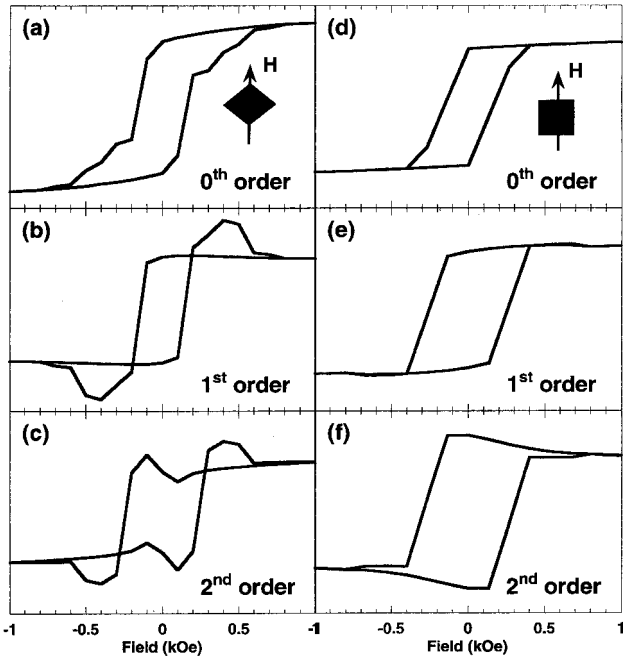

FIG. 10. Hysteresis loops for large square holes calculated using micromagnetic simulations and Eqs. (1) and (2). (a)–(c) are for a field along the diagonal. (d)–(f) are for a field parallel to an edge.

square holes, do not produce an acceptable description of the results for large holes. In hindsight this can be understood on the basis that such ''band'' domains would have domain walls at large angles to the magnetization bisector and hence would introduce large dipolar energies. An alternative domain structure for this direction of the applied field, constructed so as to satisfy the energy constraints described above, is shown in Fig. 8. The corresponding form factors are given in Table II. They predict −20%, −45%, and +26% changes in the zeroth-, first-, and second-order loops, providing a reasonable qualitative description of the loops in Figs. 7(d)–7(f).

We have been unable to find a simple domain structure (i.e., one based on the domains in Fig. 5) that can account for the loops in Figs. 7(a)–7(e). This may simply be an indication that suitable domain structures have been missed in our analysis, that the simplifications involved in such an approach are not valid for this configuration or that the domain structure is indeed more complex than those based on simple arguments.

IV. MICROMAGNETIC SIMULATIONS

Micromagnetic simulations yield the equilibrium spin configuration of an object subjected to an external field. From the spin configuration it is easy to calculate the form factors of any order [Eq. (1)] and then, via Eq. (2), calculate the corresponding hysteresis loops. While attempting to use the NIST code[10] to investigate the magnetization profiles in our hole arrays, we have encountered a number of difficulties. The most serious is that the code, in its present form, does not allow the introduction of suitable boundary conditions necessary to deal with an extended (infinite) structure. In the absence of the correct boundary conditions the edges of a structure introduce many serious artifacts into the calculation: edges enhance magnetization rotation when M is perpendicular to them and hinders its rotation when M is parallel to an edge. The resulting spin structures that appear during reversal are consequently not determined by the holes but by the edges themselves.

The edge problem can be reduced somewhat by performing calculations on a structure consisting of many unit cells. If enough cells are included one may expect the central cells to respond in a manner equivalent to an infinite sample. The

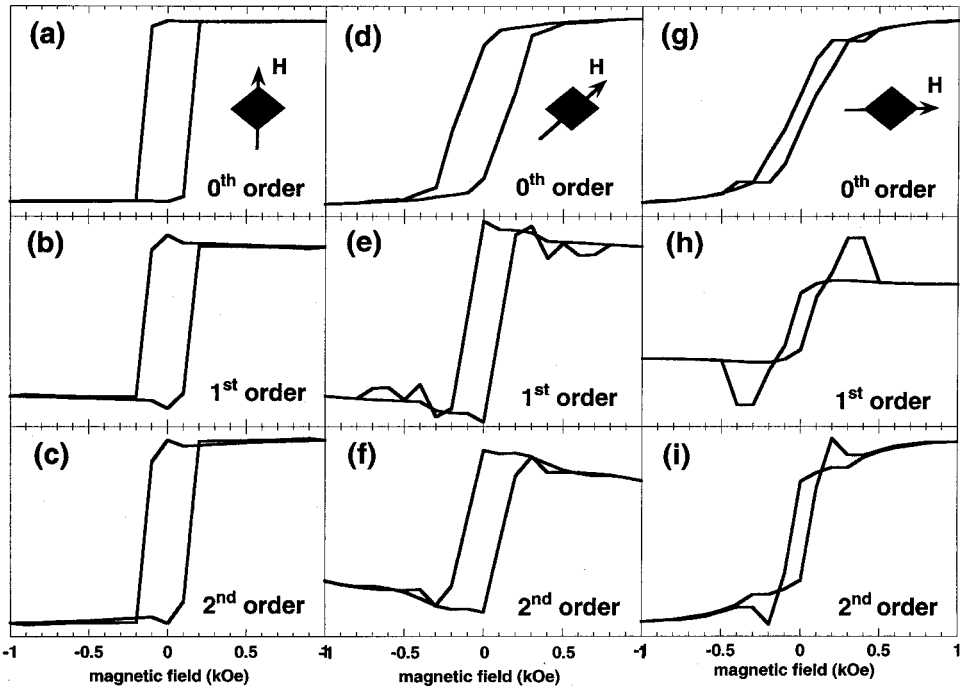

FIG. 11. Hysteresis loops for small square holes calculated using micromagnetic simulations and Eqs. (1) and (2). (a)–(c) are for a field along a diagonal (easy axis). (d)–(f) are for a field parallel to an edge. (g)–(i) are for a field along a diagonal (hard axis).

competing requirements of reasonable simulation times, and yet small enough computational elements to reproduce the hole array within a unit cell, severely restrict the number of unit cells that can be simulated. In our case only systems smaller than 5×5 unit cells could be undertaken. Even with such sizes it is evident that the edges still strongly influence the behavior of the central cell. The additional complications are that domain formation can depend strongly on the exact direction of the applied field and also on the magnitude and direction of anisotropy in the film. The convergence criterion used in the simulation can also dramatically affect the resulting configurations especially in the vicinity of the reversal. On the other hand, stringent conversion parameters invariably lead to unrealistic simulation times.

We succeeded in further reducing the effect of the edges by ''roughening'' them. This was accomplished by removing half the computational cubes from around the edges of our 5×5 structure. With this ploy the domain structure in each of the central nine cells is usually quite similar indicating that the central cell is indeed well ''isolated'' from the edges. In these cases we found that the domain patterns proposed in Figs. 6 and 8 do indeed appear during reversal. In Fig. 9, we show some configurations that appeared during simulations at fields close to the switching field. Figures 9(a) and 9(b) show ''band'' domains similar to those we propose in Figs. 6(a) and 8, respectively. The structures shown in Figs. 9(c) and 9(d) are consistent with the domains proposed in Figs. 6(b) and 6(c), respectively.

At any given field the form factors can be extracted from the micromagnetic simulations. For the sample with large holes these field-dependent form factors, for two different field directions, produce the hysteresis loops shown in Fig. 10. These loops exhibit features very closely resembling the loops in Fig. 7. Note, however, that even though the basic loop shapes are reproduced, the calculated coercivity is almost twice the experimental value. It is clear that further work is required to understand the details and limitations of the simulations. It may of course be due to the fact that the real samples contain imperfections not included in the simulations.

Similar micromagnetic simulations for the small holes, in which we included anisotropy, are shown in Fig. 11. Again the basic shapes of the loops are in good agreement with those in Fig. 4. However, the simulations that lead to loops in Figs. 11(g)–11(i) did not yield the same domain structure in all the central cells. In particular, the loops presented in Figs. 11(g)–11(i) do not correspond to the central cell but to an adjoining cell that exhibited the structure proposed in Fig. 6(c). The form factors from other cells did not produce agreement with the loops in Fig. 4. In this sense the micromagnetic results have been biased in favor of the simple picture presented in the preceding section, again indicating that further work is necessary to achieve full confidence in the simulations.

V. RESULTS: MFM

In the course of this investigation we also investigated our samples with MFM. Although instrumental resolution was not optimum, the instrument allowed measurements to be performed with externally applied fields. As expected, at fields close to saturation all hole array samples showed bright and dark regions at the hole edges. On reducing the applied fields contrast became weaker and, at remanence, most samples produced MFM images with no clearly defined structures.

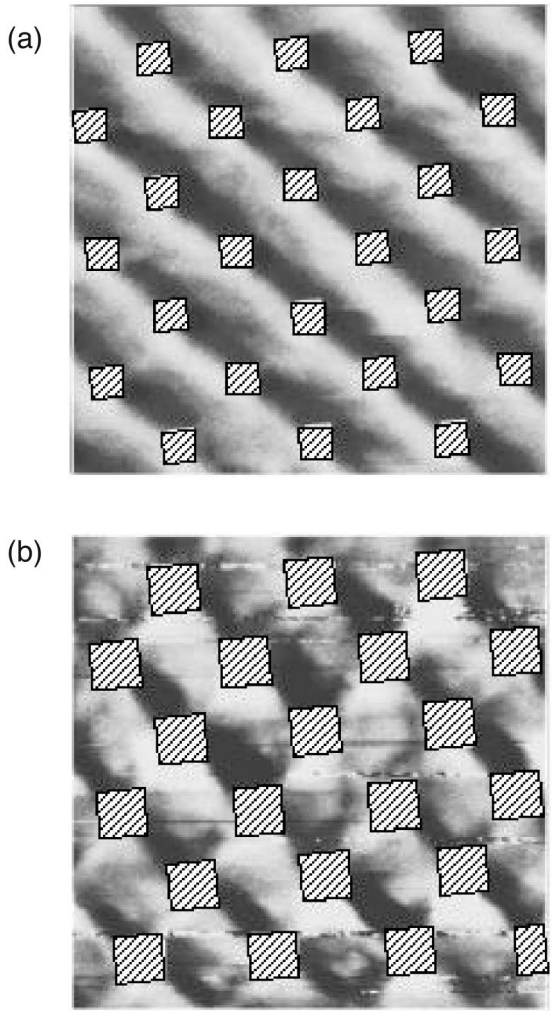

FIG. 12. $5\times5\ \mu m^2$ MFM images of the remnant state of the sample with small square holes (upper) and large square holes (lower).

One particularly interesting case was the sample with elliptical holes investigated in Ref. 8. In that sample we know that domains are present at remanence since it was shown by both DMOKE and Lorentz microscopy, that the domains form bands similar to those in Fig. 6(a). The preceding observation can be understood by recalling that the force detected by MFM is due to the ''magnetic charges'' that appear when the divergence of the magnetization is nonzero. At saturation, bright and dark regions are expected at the hole edges as observed experimentally. When domains form it is necessary to consider the ''charge'' at each domain wall. As mentioned earlier, however, one of the driving forces during domain formation is the reduction of dipolar energy achieved by placing the normal of a domain wall along the bisector of

the magnetization directions. In this approximation the domain patterns shown in Figs. 5(a), 5(c), and 5(e) would show no contrast in MFM images. Because the domains walls in the sample with elliptical holes,[8] and the domains in Fig. 6(c), which explain the DMOKE loops in Figs. 4(g)–4(i), are, by symmetry, exactly along the bisector of adjacent magnetization directions, no contrast is expected in the corresponding MFM images.

It is only when a domain wall is no longer along the magnetization bisector that contrast is expected in MFM images. In this context, the domains in Figs. 5(b) and 5(d) would produce a contrast proportional to their deviation from the domains in Figs. 5(a) and 5(c). Also, the domains in Fig. 6(b) will produce only a weakening and some smearing compared to the image at saturation.

The only MFM image that showed a clear structure was obtained for the small holes and is shown in Fig. 12(a); it is compatible with the domains in shown Fig. 6(a). The white squares in the image have been transferred from the atomic force microscopy image and added for clarity to show the position of the holes. The reason for the contrast is that the domain walls in Fig. 6(a) are not along the bisector of the magnetizations and hence should contain ''magnetic charges.'' Why the slight zigzagging is not observed may be due to the resolution of the MFM image itself.

Figure 12(b) shows the MFM image of the array of large square holes recorded at remanence. Extracting domain structure from this image is clearly unreliable, again emphasizing the caveats associated with interpreting MFM images.

VI. CONCLUSIONS

Magnetic anisotropy and domain formation in arrays of square holes in an Fe film have been investigated using MOKE, Brillouin scattering, DMOKE, micromagnetic simulations, and MFM. The uniaxial anisotropy of the unpatterned film is found to persist in the patterned regions but an additional fourfold anisotropy, induced by the square holes, is also observed. Since no array-induced anisotropy was reported for an array of round holes on a square lattice,[7] and a uniaxial anisotropy was observed in an array of elliptical holes on a square lattice,[8] we conclude that it is the shape of the holes and not the symmetry of the lattice that determines the anisotropy.

Domain formation is monitored using DMOKE. Hysteresis loops measured on various diffraction orders are interpreted in terms of the ''form-factor'' model presented in Ref. 8. Although it is not possible to invert the DMOKE information to extract the domain structure, it is possible to construct energy-constrained domain patterns and to test their viability against the DMOKE loops. For the two samples investigated here, square holes of two different sizes on a square lattice, we find domain structures that qualitatively reproduce the shapes of the DMOKE loops. Minor discrepancies are attributed to the finite wall thickness and to inhomogeneous domain formation across the array.

Micromagnetic simulations are found to suffer from large ''edge effects.'' However, the simulation of large areas with roughened edges greatly reduces the deleterious effects of the edges and lead to results in good agreement with the experiment. MFM techniques are found to provide little insight into the reversal mechanism in hole arrays.

Work at ANL was supported by the US Department of Energy, BES, and Materials Science under Grant No. W-31-109-ENG-38. I.G. wishes to acknowledge DF/UFC and CNPq for support during his stay at ANL. V.M. acknowledges support under NSF Grant No. ECS-0202780. P.V. acknowledges support from INFM under the ''MAGDOT'' PAIS program and MURST-COFIN 2000. We acknowledge Dr. O. Donzelli for access to the MFM instrument.

*Present address: Departments de fisica, UFC Caixa Postal 6030, Campus do Pici 60455-760, Fortaleza, CE, Brazil.

†Visiting scientist at MSD ANL, summer of 2001.

[1] C. A. Grimes, P. L. Trouilloud, J. K. Lumpp, and G. C. Bush, J. Appl. Phys. **81**, 4720 (1997).

[2] R. P. Cowburn, A. O. Adeyeye, and J. A. Bland, Appl. Phys. Lett. **70**, 2309 (1997); J. Magn. Magn. Mater. **173**, 193 (1997).

[3] Y. Otani, S. G. Kim, T. Kohda, K. Fukamichi, O. Kitakami, and Y. Shimada, IEEE Trans. Magn. **34**, 1090 (1998).

[4] L. Torres, L. Lopez-Diaz, and J. Iñiguez, Appl. Phys. Lett. **73**, 3766 (1998).

[5] L. Torres, L. Lopez-Diaz, O. Alejos, and J. Iñiguez, J. Appl. Phys. **85**, 6208 (1999).

[6] C. T. Yu, H. Jiang, L. Shen, P. J. Flanders, and G. J. Mankey, in *Proceedings of the 44th Annual Conference on Magnetism and Magnetic Materials* [J. Appl. Phys. **87**, 6322 (2000)].

[7] P. Vavassori, V. Metlushko, R. M. Osgood, M. Grimsditch, U. Welp, G. Crabtree, W. Fan, S. Brueck, B. Ilic, and P. Hesketh, Phys. Rev. B **59**, 6337 (1999).

[8] I. Guedes, N. J. Zaluzec, M. Grimsditch, V. Metlushko, P. Vavassori, B. Ilic, P. Neuzil, and R. Kumar, Phys. Rev. B **62**, 11 719 (2000).

[9] J. Sandercock, in *Light Scattering in Solids III*, edited by M. Cardona and G. Güntherodt, Topics in Applied Physics Vol. 51 (Springer, New York, 1982).

[10] M. J. Donahue and D. G. Porter, OOMMF User's Guide, Version 1.0 (National Institute of Standards and Technology, Gaithersburg, MD, 1999) http://math.nist.gov/oommf/

[11] S. Chicazumi and S. Charap, *Physics of Magnetism* (Wiley, New York, 1964).

[12] H. J. Williams, R. M. Bozorth, and W. Shockley, Phys. Rev. **75**, 155 (1949).

[13] L. Néel, Cah. Phys. **25**, 21 (1944).